# Extraction of Transformer Saturation Curve from Ferroresonance Measurements Based on Nelder–Mead Optimization Method

V. Milardić, A. Tokić, I. Uglešić, A. Xemard

***Abstract*--An accurate representation of the transformer saturation curve is essential for calculations of low frequency transients (inrush current, ferroresonance, load rejection) and steady states (power quality problems, harmonics and subharmonics). This paper presents an original extraction methodology for determining the transformer saturation curve from the measured ferroresonant current and voltage waveforms. The proposed method is based on the formulation of a novel multiobjective function, using current and voltage obtained from the measurement. The proposed simulation-optimization method is based on the Backward Differentiation Method for solving the very stiff differential equation system that describes the ferroresonance as well as the Nelder-Mead optimization method used to minimize the proposed multiobjective function. Five functions are proposed for approximating the saturation curve. The best ferroresonance simulation results are obtained with the inverse extended Frolich function. The validity of the proposed methodology has been confirmed by a very good agreement between the measured and simulated results of the ferroresonant current and voltage under different ferroresonance scenarios (three different values of series capacitances).**

***Keywords*: Saturation curve, ferroresonance, Backward Differentiation Method, Ordinary Differential Equation System, Nelder-Mead optimization method, transformer modelling.**

## I. Introduction

HIGH–FIDELITY modelling of transformer saturation curve is an essential subject in simulations of low-frequency electromagnetic transients (ferroresonance, inrush current, geomagnetic-induced currents) and simulations of steady-states (harmonics, power quality).Piece-wise saturation curve magnetizing current–flux linkage ($i_m$–$\phi$) is usually obtained by conversion from the RMS current-voltage curve ($I_{RMS}$–$U_{RMS}$) using the procedures shown in [1]-[3]. The RMS curve is provided by the manufacturer or obtained by measurements. However, the standard no-load test given by the manufacturer is usually limited to only a few points i.e. the iron core is not driven into deep saturation and may lead to significant errors in simulations of the ferroresonance. In addition, measurements of the saturation curve are limited as they can sometimes lead to overheating of the windings and core, as well as excessive stress of the transformer insulation. Based on the above, it can be stated that there is still a need for correct modelling of the transformer saturation curve, which is the dominant subject of this paper.

The extraction of the saturation curve is mainly obtained from the inrush current test. In paper [4] only the first inrush current peak is used for the estimation procedure and in paper [5] several cycles of the inrush current are used. A very simplified analytical method for the conversion of the current-time curve into the current-flux curve, based on signal samples idealization of the peak inrush current, was proposed in paper [6]. In paper [7], the parameters of the saturation curve are obtained by the direct method from the waveforms of the no-load and inrush currents. The problem is that in these works the developed transformer model is tested only for one scenario of inrush current. In papers [8]-[10], some optimization methods are presented for estimating the linear parameters of the transformer, which ignore the nonlinear character of the saturation curve, so that they are not at all suitable for simulations of the ferroresonance.

In ferroresonance simulations, the transformer nonlinear saturation curve is predominantly represented by piece-wise linear regions [11] or by polynomial functions (two or three terms) [12]-[16]. When representing the saturation curve by two-terms polynomials, it is very important to obtain the correct values for the polynomial coefficients.

The nonlinear saturation curve of the transformer can be determined from ferroresonance measurements, however, as far as the authors are aware, there are no papers demonstrating that. This is because, in the case of a single-phase transformer series ferroresonance with a sufficiently large capacitance value, large current values are achieved, so that the transformer is drawn into deep saturation. During single-phase ferroresonance, two time-dependent variables can be measured directly: ferroresonant current and voltage, while during transformer energization, only the inrush current can be measured. The simultaneous extraction of the saturation curve from two state variables is mathematically more correct than the extraction from only one variable (transformer current).

The focus of this work is to develop an algorithm (methodology) for parameter extraction of the saturation curve of a single-phase transformer using simultaneously measured ferroresonant current and voltage waveforms. The modelling and simulation of the ferroresonance is based on the solution of the system of ordinary differential equations (ODE), using a

V. Milardić and I. Uglešić are with University of Zagreb Faculty of Electrical Engineering and Computing, Croatia (viktor.milardic@fer.hr, ivo.uglesic@fer.hr)
A. Tokić is with University of Tuzla, Faculty of Electrical Engineering, Tuzla, Bosnia and Herzegovina (amir.tokic@untz.ba)
A. Xemard is with EDF France (alain.xemard@edf.fr )
Paper submitted to the International Conference on Power Systems Transients (IPST2023) in Thessaloniki, Greece, June 12-15, 2023.

suitable Backward Differentiation Method (BDF) [17]. Parallel to solving the ODE system, the extraction of saturation curve parameters is achieved using the heuristic Nelder–Mead method to optimize the proposed original multiobjective function that incorporates ferroresonant current and voltage waveforms. To validate the proposed methodology, a comparison is made between the simulation and measurement results for different modes of ferroresonance.

The rest of this paper is structured as follows. Section II presents the modelling, simulation and optimization procedure in a single-phase serial ferroresonant circuit. Section III presents the application of the proposed methodology for extraction of transformer saturation curve. Section IV demonstrates the validation of the obtained optimization results. Finally, Section V concludes the paper.

## II. Ferroresonant Circuit Modelling, Simulation and Optimization

Ferroresonance is a well-known nonlinear dynamic phenomenon that occurs in electrical systems containing an iron core inductor and capacitor excited by an arbitrary supply source voltage. It represents an oscillating energy exchange between iron core inductors (magnetic field energy) and capacitors (electric field energy). Ferroresonace leads to the occurrence of distorted overvoltages and overcurrents in a system, which can be harmful to the system components. This phenomenon leads to one of the following four modes: (a) fundamental mode, (b) subharmonic mode, (c) pseudoharmonic mode and (c) chaotic mode [12].

The model shown in Figure 1 is the most common representation of a serial ferroresonant circuit. The linear elements of the single-phase two-winding transformer model are: $R_p$, $R_s$ primary and secondary winding resistance, $L_p$, $L_s$ primary and secondary winding inductance, $R_m$ core loss resistance, $L_m$ represents the non-linear inductance of the iron core of the transformer. All linear elements mentioned are obtained by standard short-circuit and no-load tests.

Figure 1 also shows the following parameters: $e(t)$ source voltage, $C$ series capacitor, $i(t)$ transformer ferroresonant current, $u(t)$ transformer ferroresonant voltage, $i_m$ magnetizing current, $\phi$ magnetic flux, and $N_p : N_s$ transformer turns ratio.

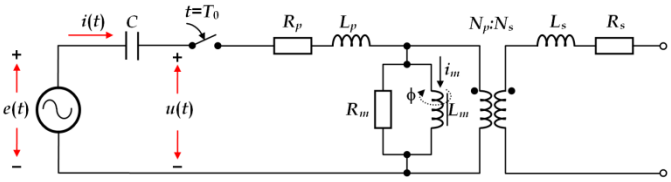


Fig. 1. Ferroresonant circuit model

In the previous part of the text, it was already pointed out that the non-linear saturation curve can be modelled by piecewise linear regions. However, due to the above-mentioned limitations in laboratory measurements, it remains questionable to determine the last linear region (the last slope) in deep saturation.

On the other hand, problems of overshooting and non-differentiability of the proposed functions could arise when representing the saturation curve by piecewise linear regions [18]-[19].

The mentioned problems are eliminated by modelling the saturation curve using nonlinear analytical functions. One of the main goals of this work is the parameter extraction and comparative analysis of some representative analytical functions that model the nonlinear transformer saturation curve in ferroresonance analyses.

### A. State-Space Equation for Ferroresonant Circuit

The following nonlinear state-space equation describing the transformer transient during a serial ferroresonance analysis is developed in the following form:

$$\frac{dX}{dt} = F(X, t, \Lambda) \tag{1}$$

where state vector $X = \begin{bmatrix} u_C & i & \phi \end{bmatrix}^{\mathrm{T}}$ and system matrix:

$$F(X,t,\Lambda) = \begin{bmatrix} \frac{1}{C} i \\ -\frac{1}{L_p} u_C - \frac{R_p + R_m}{L_p} i + \frac{R_m}{L_p} i_m(\phi, \Lambda) + \frac{1}{L_p} e(t) \\ R_m i - R_m i_m(\phi, \Lambda) \end{bmatrix} \tag{2}$$

In equation (1),the unknown parameters in the analytical function that models the nonlinear saturation curve is defined by the vector $\Lambda = \begin{bmatrix} \lambda_1 & \lambda_2 & \dots & \lambda_n \end{bmatrix}^{\mathrm{T}} \in R^n$.

The numerical properties (stiffness ratios and stiffness indexes) of the differential equation systems describing the low-frequency transformer transients such as serial ferroresonance and inrush currents show that these equations represent very stiff equation systems [20]-[21]. It is not possible to solve them by applying classical explicit numerical methods. Therefore, it is necessary to apply implicit numerical methods, which are characterized by special properties in terms of numerical accuracy and numerical stability.

For solving equation (2), a multistep BDF method of order $p$ is proposed:

$$G(X_{k+1}, \Lambda) = \sum_{m=1}^{p} \frac{1}{m} \nabla^m X_{k+1} - \Delta t F(X_{k+1}, t_{k+1}, \Lambda) = 0 \tag{3}$$

The equation (3) is solved by Newton-Raphson method:

$$X_{k+1}^{l+1} = X_{k+1}^{l} - \left[ G'_{X_{k+1}}(X_{k+1}^{l}, \Lambda) \right]^{-1} \cdot G(X_{k+1}^{l}, \Lambda) \tag{4}$$

where $k$=1,2,... is a number of integration steps of the BDF ODE method of order $p$, while $l$ = 1,2,... is a number of iterations of the Newton-Raphson method within each integration step.

In the relation (4), the Jacobian 3×3 matrix as ($E$– eye 3×3 matrix) is obtained:

$$J(X_{k+1},\Lambda)=G'_{X_{k+1}}(X_{k+1},\Lambda)=\sum_{m=1}^{p}\frac{1}{m}\cdot E-\Delta t\cdot\frac{\partial F(X_{k+1},t_{k+1},\Lambda)}{\partial X_{k+1}} \quad (5)$$

The particular value of the matrix $G$ can be obtained by:

$$G(X_{k+1}^{l},\Lambda)=\sum_{m=1}^{p}\frac{1}{m}\nabla^{m}X_{k+1}^{l}-\Delta t F(X_{k+1}^{l},t_{k+1},\Lambda)=0 \quad (6)$$

Considering the state-space equation (1), the following matrices are obtained that describe the solution of the ferroresonant system are obtained:

$$F(X_{k+1}^{l},t_{k+1},\Lambda)=\begin{bmatrix}\frac{1}{C}i_{k+1}^{l}\\ -\frac{1}{L_p}u_{C_{k+1}}^{l}-\frac{R_p+R_m}{L_p}i_{k+1}^{l}+\frac{R_m}{L_p}i_m(\phi_{k+1}^{l},\Lambda)+\frac{1}{L_p}e_{k+1}\\ R_m i_{k+1}^{l}-R_m i_m(\phi_{k+1}^{l},\Lambda)\end{bmatrix} \quad (7)$$

$$\frac{\partial F(X_{k+1}^{l},t_{k+1},\Lambda)}{\partial X_{k+1}}=\begin{bmatrix}0 & \frac{1}{C} & 0\\ -\frac{1}{L_p} & -\frac{R_p+R_m}{L_p} & \frac{R_m}{L_p}\frac{\partial i_m(\phi_{k+1}^{l},\Lambda)}{\partial\phi}\\ 0 & R_m & -R_m\frac{\partial i_m(\phi_{k+1}^{l},\Lambda)}{\partial\phi}\end{bmatrix} \quad (8)$$

It should be noted that for solving the state-space equation (1) it is most convenient to use the BDF method of order 2, since this method has the special features of accuracy (second order method) and stability ($A$ and $L$ stable method) [22]-[23].

### *B. Application of Nelder–Mead optimization method for extraction of saturation curve*

As it can see from Figure 1, the basic observed quantities are the ferroresonant current ($i$) and the ferroresonant transformer voltage ($u$). These two quantities have different units and represent completely different waveforms, i.e. they have different peak values and corresponding harmonic content.

Due to the different range of the state variables ($i$) and ($u$), it is necessary to formulate a special multiobjective function suitable for the qualitative extraction of the transformer saturation curve parameters.

In this context, this paper proposes individual objective functions related to the ferroresonant current and voltage:

$$f_1(\Lambda)=\sum_{k=1}^{N}\left(\frac{i_{\text{sim.}}(k,\Lambda)-i_{\text{meas.}}(k)}{\|i_{\text{meas}}\|_2}\right)^2 \quad (9)$$

$$f_2(\Lambda)=\sum_{k=1}^{N}\left(\frac{u_{\text{sim.}}(k,\Lambda)-u_{\text{meas.}}(k)}{\|u_{\text{meas}}\|_2}\right)^2 \quad (10)$$

where Euclidean 2–norms are:

$$\|i_{\text{meas}}\|_2=\left(\frac{1}{N}\sum_{k=1}^{N}i_{\text{meas.}}^2(k)\right)^{1/2},\quad \|u_{\text{meas}}\|_2=\left(\frac{1}{N}\sum_{k=1}^{N}u_{\text{meas.}}^2(k)\right)^{1/2}$$

Finally, it is suggested multiobjective objective function as arithmetic mean of these scaled individual functions:

$$f(\Lambda)=\frac{1}{2}\left[f_1(\Lambda)+f_2(\Lambda)\right] \quad (11)$$

The individual objective functions $f_1$ and $f_2$ are normalized by their corresponding values of the Euclidean 2 - norm. This ensures a balance in the contribution of the individual objective functions. The minimization of this function with respect to the vector $\Lambda$ gives the corresponding parameters of the analytical function used to model the transformer saturation curve.

To find the minimum value of the proposed multiobjective function $F(\Lambda)$, the Nelder–Mead optimization method [24] is recommended in this paper. The Nelder–Mead method is a heuristic optimization technique commonly used to determine the minimum of a multiobjective function $F(\Lambda)$, $\Lambda\in R^n$ in $n$-dimensional vector space. This method represents a nun constrained direct search method which relies on the geometrical construction of a specially defined convex simplex ($S$) of $n$+1 vertices, for an $n$ –dimensional problem. This method, through a particularly defined strategy, iteratively replaces its vertices for new ones with lower values of the objective function. During each iteration, the method always starts by calculating a reflected point of the worst point by defining the centroid point. Using this value, Nelder–Mead algorithm performs special operations: (a) reflection or extension, (b) contraction or shrink to generate a new simplex ($S$). The objective function values at each vertex evaluates in each iteration and the worst vertex with the highest value will be replaced by another vertex which has just been found. Otherwise, the simplex ($S$) will be shrunk around the best determined vertex. The reduction of the simplex ($S$) leads to convergence of the method (of all simplex points) towards the final optimal solution. Details of the properties of Nelder–Mead optimization method (derivation, convergence, implementation) are presented in the references [24]-[26]. The main advantage of this method is its independence from the gradient of the objective function or any approximation. This means that it is applicable to non-differentiable (non-smooth or discontinuous at certain points) functions or to cases where the gradient of the objective function is unknown. These properties make it more efficient and robust compared to the traditional optimization methods [24], [26], [28].

It should be noted that there are other optimization methods suitable for electromagnetic transient problems. In this regard, the Kriging method [27], Levenberg-Marquardt algorithm, trust-region method, conjugate gradient method and quasi Newton method [24] can be singled out. Each of the mentioned methods has its own advantages and disadvantages, depending on the specific problem being analyzed. Thus, for example, the paper [27] presents the application of the Kriging method to the design of the automatic reactive power regulator

controller of a STATCOM.

The initial vector of the proposed optimization method is particularly important, and the procedure for its calculation is presented in the next part of the paper. The initial vector of the optimization method $\Lambda_0$ is calculated by using the non-linear least squares method (NLSM) with the proposed analytical function $i_m = i_m(\phi, \Lambda)$, for the single valued curve: the measured ferroresonant current $i_{meas.}(t)$, vs. flux $\phi_{meas.}(t)$, as the calculated integral of the measured ferroresonant voltage $u_{meas.}(t)$. Both quantities $i_{meas.}(t)$ and $\phi_{meas.}(t)$ are defined in the time interval between the zero value of the ferroresonant current and the first peak of the ferroresonant current $[t_{zero}, t_{peak}]$ (marked in Figures 2 and 3). From measured ferroresonant voltage $u_{meas.}(t)$, using the trapezoidal method of integration with appropriate time step $\Delta t$, it was calculated the flux $\phi_{meas.}(t)$:

$$\phi_{meas.}(t) = \phi_{meas.}(t - \Delta t) + \frac{\Delta t}{2}\left[u_{meas.}(t - \Delta t) + u_{meas.}(t)\right] \quad (12)$$

The obtained tabulated values: measured current and calculated flux are:

$$i_1 = i_{meas.}(t_{zero}),\ i_2 = i_{meas.}(t_{zero} + \Delta t),\ ...,\ i_{j\max} = i_{meas.}(t_{zero} + p_{max}\Delta t) \quad (13)$$

$$\phi_1 = \phi_{meas.}(t_{zero}),\ \phi_2 = \phi_{meas.}(t_{zero} + \Delta t),\ ...,\ \phi_{j\max} = \phi_{meas.}(t_{zero} + p_{max}\Delta t) \quad (14)$$

where is: $p_{max} = (t_{peak} - t_{zero})/\Delta t$ the total number of samples.

Finally, NLSM is applied to the obtained data series $\{i_j, \phi_j\}$, $j = 1, 2, \ldots, j_{max}$, using the appropriate analytical function $i = i(\phi, \Lambda_0)$, $\Lambda_0 = [\lambda_{10}, \lambda_{20}, ..., \lambda_{n0}]^T$.

## III. Extraction of Saturation Curves by Applications of Proposed Methodology

The proposed methodology for extraction of saturation curve will be applied to the serial (240/39 *V*) transformer ferroresonant circuit shown in Figure 1. The electrical system parameters are:

- transformer rated power: 350 *VA*,
- source voltage: $e(t) = 345\sin(\omega t - 89.05°)$,
- winding resistance: $R_p = 3.10\Omega$,
- leakage inductance: $L_p = 11.5\ mH$,
- core-loss resistance: $R_m = 4324\Omega$,
- serial capacitance: $C = 10\ \mu F$.

To eliminate the impact of the transformer's residual flux and the capacitor's initial voltage, the transformer was demagnetized ($\phi_{rem} = 0$) and the capacitor was completely discharged ($u_{C0} = 0$) before the breaker was switched-on.

It should be noted that the maximum value of the capacitance $C_{max.} = 10\ \mu F$ was chosen, which ensures the entry of the transformer in deep saturation. On the other hand, $C_{max.}$ is the capacitance value at which the transformer and capacitor could still withstand the thermal and voltage stresses of the insulation when establishing very high ferroresonant overcurrent and overvoltage in the electric circuit. The measurement results of the transformer ferroresonant current and voltage waveforms, which represent the input data for the proposed extraction methodology are given in Figures 2 and 3.

In addition, network voltage waveform $e(t)$ is also known as input data. A good feature of the measured signals from Figures 2 and 3 is that in the observed windows of 0.2 s, a stationary state is reached, which enables better extraction of the approximation functions that will be used in this paper.

The nonlinear analytical functions: three-term polynomial, two-term hyperbolic, three-term exponential, inverse extended Frolich, and five-term irrational (marked by: # *l*, *l* = 1, 2, ..., 5) shown in Table I, were taken for the representative functions. Due to space limitations, this paper presents the optimization results for only five (5) proposed analytic functions, although some others, less accurate analytic functions were also tested. For example: two-term polynomial, original Frolich function, logarithmic function, two-term exponential function etc.

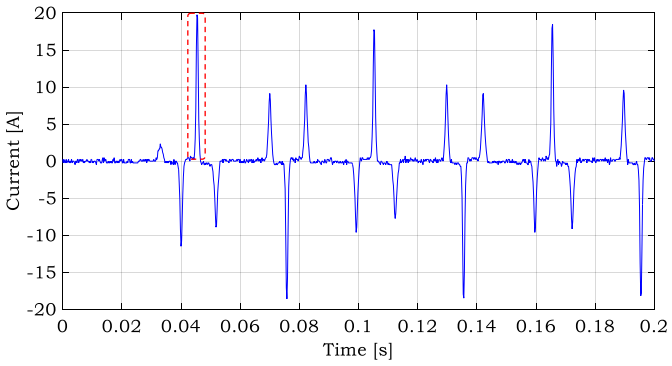


Fig. 2. Measured transformer ferroresonant current, $C = 10\ \mu F$

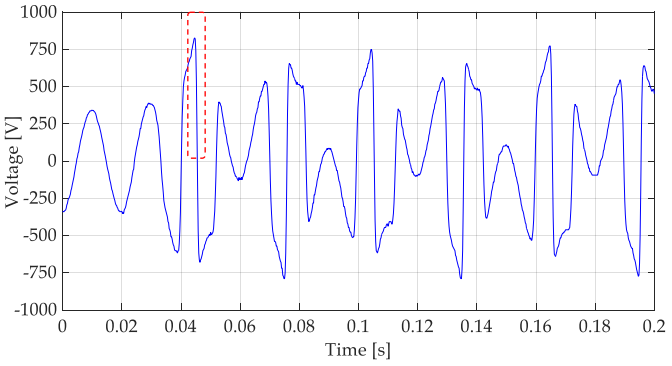


Fig. 3. Measured transformer ferroresonant voltage, $C = 10\ \mu F$.

Table II shows the results of the proposed optimization methodology for the representative analytical function. This Table shows the optimization results for scaled individual objective functions $F_1$ and $F_2$ as well as for the total multiobjective function $F$.

Finally, Table III shows the results, according to the NLS method, of the calculated initial vector $\Lambda_0$ as well as the results of the final vector $\Lambda_{final}$ of unknown parameters that define the proposed nonlinear analytical saturation curves.

According to the results shown in Table III, the following Figure 4 shows the transformer saturation curve optimization results, extracted by using the final multiobjective function $F$ with the proposed Nelder–Mead method. This Figure additionally shows the extrapolated piece-wise saturation curve obtained by converting the RMS curve from the standard no-load transformer test. It is clear that this piece-

wise curve has a high last slope, which makes it unsuitable for simulating ferroresonance with high values of currents and voltages (large values of serial capacitance *C*).

TABLE I
REPRESENTATIVE ANALYTICAL FUNCTIONS FOR EXTRACTION OF THE SATURATION CURVES ( MARKED BY $\#l, l = 1,2,...,5$ )

| Function No. | Analytic function – Saturation curve |
|---|---|
| #1 polynomial | $i_m(\phi,\Lambda) = \lambda_1\phi^{\theta_1} + \lambda_2\phi^{\theta_2} + \lambda_3\phi^{\theta_3}$ |
| #2 hyperbolic | $i_m(\phi,\Lambda) = \lambda_1 \sinh(\lambda_2\phi)$ |
| #3 exponential | $i_m(\phi,\Lambda) = \phi\left(\lambda_1 + \lambda_2 e^{\lambda_3\lvert\phi\rvert}\right)$ |
| #4 inverse Frolich extended | $\phi(i_m,\Lambda) = \dfrac{i_m}{\lambda_1 + \lambda_2\lvert i_m\rvert + \lambda_3\sqrt{\lvert i_m\rvert}}$ |
| #5 irrational | $F(i_m,\phi,\Lambda) = \text{sign}(\phi)\left[\lambda_1 i_m + \text{sign}(\phi)\lambda_2 - \phi\right]\cdot \left[\lambda_3 i_m + \text{sign}(\phi)\lambda_4 - \phi\right] - \text{sign}(\phi)\cdot\lambda_2\lambda_4 - \lambda_5\phi = 0$ |

TABLE II
RESULTS OF OPTIMIZATION FOR SCALED INDIVIDUAL OBJECTIVE FUNCTIONS AND TOTAL MULTIOBJECTIVE FUNCTION

| No. | $f_1(\Lambda_{final})$ | $f_2(\Lambda_{final})$ | $f(\Lambda_{final})$ |
|---|---|---|---|
| #1 | 1.4817 | 2.3273 | 1.9045 |
| #2 | 1.8497 | 3.0110 | 2.4303 |
| #3 | 1.4774 | 2.4809 | 1.9792 |
| #4 | 0.9472 | 1.5313 | 1.2393 |
| #5 | 1.2444 | 1.2385 | 1.2414 |

TABLE III
RESULTS OF OPTIMIZATION FOR SCALED INDIVIDUAL OBJECTIVE FUNCTIONS AND TOTAL MULTIOBJECTIVE FUNCTION

| No. | Initial vector $-\Lambda_0$ | Final solution $-\Lambda_{final}$ |
|---|---|---|
| #1 | $\Lambda_0 = \begin{bmatrix} 0.2793 \\ 0.1615 \\ 0.0286 \end{bmatrix}$ | $\Lambda_{final} = \begin{bmatrix} 0.0673 \\ -0.0194 \\ 0.1313 \end{bmatrix}$ |
| #2 | $\Lambda_0 = \begin{bmatrix} 0.0024 \\ 5.4420 \end{bmatrix}$ | $\Lambda_{final} = \begin{bmatrix} 0.0002 \\ 7.8029 \end{bmatrix}$ |
| #3 | $\Lambda_0 = \begin{bmatrix} 0.1801 \\ 0.0014 \\ 5.0220 \end{bmatrix}$ | $\Lambda_{final} = \begin{bmatrix} 0.0237 \\ 0.0001 \\ 7.1784 \end{bmatrix}$ |
| #4 | $\Lambda_0 = \begin{bmatrix} 0.0010 \\ 0.4643 \\ 0.4313 \end{bmatrix}$ | $\Lambda_{final} = \begin{bmatrix} 0.0012 \\ 0.6275 \\ 0.1646 \end{bmatrix}$ |
| #5 | $\Lambda_0 = \begin{bmatrix} 23.060 \\ 0.0018 \\ -19.140 \\ 0.2731 \\ 2.6420 \end{bmatrix}$ | $\Lambda_{final} = \begin{bmatrix} 25.064 \\ 0.0039 \\ -16.331 \\ 0.4679 \\ 0.8738 \end{bmatrix}$ |

It is clear from Table II that the best optimization results were achieved by three-term inverse Frolich extended function #4 and five-term irrational function #5. Function #4 represents the dominant function for modeling the transformer saturation curve in the analyzed cases of ferroresonance (it achieves the convergence of the procedure much faster with the same range of accuracy). Function #5 has a very sharp transition from unsaturated to saturated linear region, which results in non-smooth results of state variables (small power transformer).

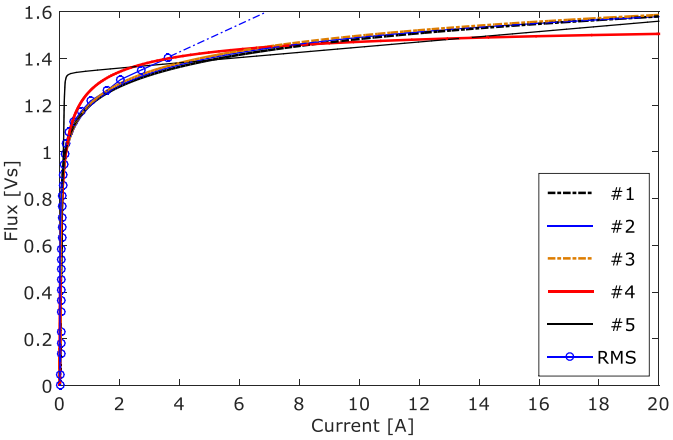


Fig. 4. Extracted saturation curves by using Nelder–Mead method: functions #*l*, *l*=1,2,...,5. RMS– curve obtained from standard no-load test

## IV. VALIDATION OF THE PROPOSED OPTIMIZATION METHODOLOGY

The proposed optimization methodology for the extraction of a saturation curve was experimentally validated on the results of ferroresonance measurements at different values of serial capacitance *C*.

The following Figures 5 and 6 show the results of the comparison between the measured and simulated transformer ferroresonant current and transformer ferroresonant voltage. Inverse extended Frolich function #4 was used to model the saturation curve. The simulations were performed by using the BDF numerical method of order two with the integration step of $\Delta t$ = 50 $\mu s$. In the mentioned Figures 5 and 6, by the value of $C$ = 10 $\mu F$, the third subharmonic mode of ferroresonance with the basic oscillation period $T$ = 60 *ms* was established in the electric circuit. It is obvious from the mentioned figures that, since the optimization procedure was realized exactly refer to these measured waveforms of current and voltage, excellent results of matching of the measured and simulated quantities (ferroresonant current and voltage) were achieved.

The obtained saturation curve by proposed optimization methodology was validated in the interpolation domain of smaller values of ferroresonant current and voltage (smaller values of serial capacitance *C*).

In this regard, Figures 7 and 8 show the results of the comparison between the measured and simulated transformer ferroresonant current and transformer ferroresonant voltage for the capacitance value $C$ = 2.5 $\mu F$. At the reduced value of the capacitance $C$ = 2.5 $\mu F$, the fundamental mode of ferroresonance with the basic oscillation period $T$ = 20 *ms* was established in the electric circuit.

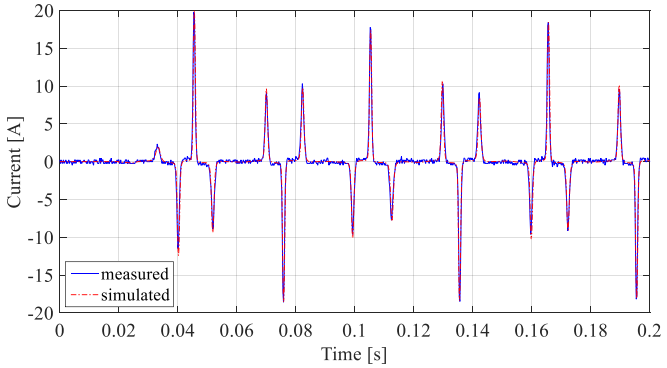


Fig. 5. Simulated vs. measured ferroresonant current, $C$ = 10 μ$F$, 3$^{th}$ subharmonic mode of ferroresonance

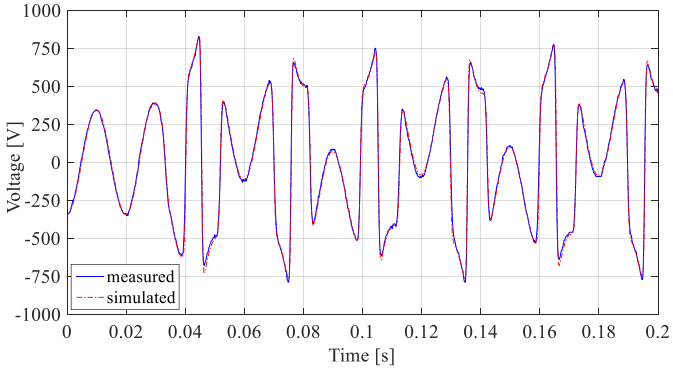


Fig. 6. Simulated vs. measured ferroresonant voltage, $C$ = 10 μ$F$, 3$^{th}$ subharmonic mode of ferroresonance

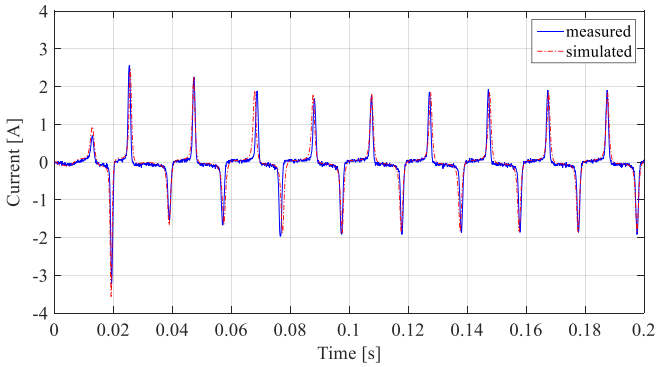


Fig. 7. Simulated vs. measured ferroresonant current, $C$ = 2.5 μ$F$, fundamental mode of ferroresonance

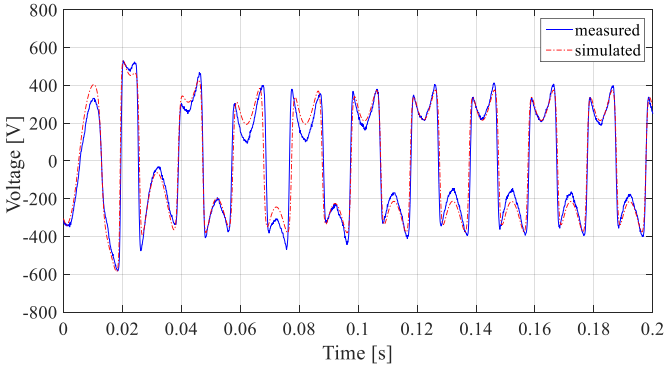


Fig. 8. Simulated vs. measured ferroresonant voltage, $C$ = 2.5 μ$F$, fundamental mode of ferroresonance

Similarly, Figures 9 and 10 show the results of the comparison between the measured and simulated transformer ferroresonant current and transformer ferroresonant voltage for an even smaller capacitance value $C$=1.2 μ$F$. Analogous to the previous case, and at this value of capacitance $C$=1.2 μ$F$, the fundamental mode of ferroresonance with the basic oscillation period $T$ = 20 $ms$ was established in the electric circuit.

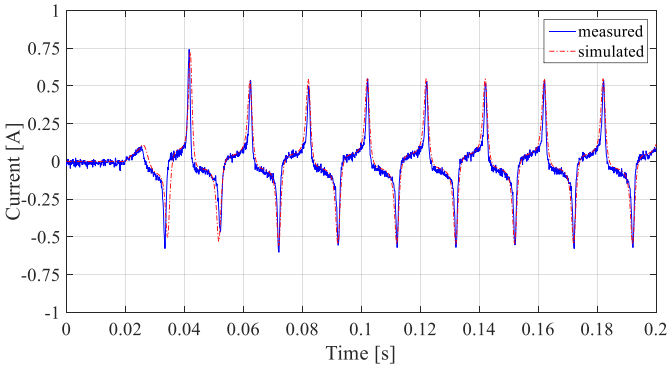


Fig. 9. Simulated vs. measured ferroresonant current, $C$ = 1.2 μ$F$, fundamental mode of ferroresonance

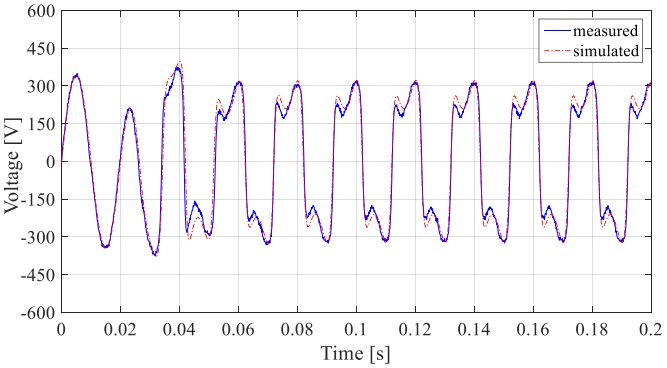


Fig. 10. Simulated vs. measured ferroresonant voltage, $C$ = 1.2 μ$F$, fundamental mode of ferroresonance

From Figures 2 to 10, it can be conclude that a very good match is achieved between the measured and simulated results of ferroresonance currents and voltages for all three different values of serial capacitance. Therefore, it is concluded that the achieved optimization results of saturation curve #4 are very good and can be used in simulations of a wide spectrum of ferroresonance, both in the domain of small values of capacitance $C$, where the fundamental mode of ferroresonance is established, as well as in the domain of large values of the capacitance $C$, where subharmonic mode of ferroresonance is established.

## V. Conclusions

This paper presents a novel methodology for parameter extraction of transformer saturation curve based on ferroresonant current and voltage measurements.

A very stiff differential equation systems that models ferroresonance is solved using the $L$-stable Backward Differentiation Formula numerical method.

To obtain the saturation curve, an original multiobjective function was proposed, which incorporates the balance

between normalized individual objective functions related to ferroresonant current and ferroresonant voltage. To find minimum value of the proposed multiobjective function, the heuristic Nelder–Mead optimization method is recommended.

Of the five proposed analytical functions used to model the saturation curve, the best results of the ferroresonance simulation were shown by the inverse extended Frolich function. The obtained simulation results, with the proposed saturation curve, for three different scenarios of ferroresonance, are validated by comparison against the corresponding measurements.

The proposed methodology for extracting the saturation curve can be further applied in simulations of low-frequency electromagnetic transients. Future research will be focused on developing a methodology for extraction of the nonlinear saturation curves for Π model of single-phase transformer and for three-phase transformers.

## VI. References


[1] J. A. Martinez, R. Walling, B. A. Mork, J. Martin-Arnedo, and D. Durbak, ‘‘Parameter determination for modeling system transients–Part III: Transformers,’’ *IEEE Trans. Power Delivery*, vol. 20, no. 3, pp. 2051–2062, Jul. 2005.

[2] W. L. A. Neves, and H. W. Dommel, “On modelling iron core nonlinearities,” *IEEE Trans. Power Systems*, vol. 8, no. 2, pp. 417–424, May 1993.

[3] A. Tokić, V. Milardić, M. Kasumović, and D. Demirović, “Conversion of RMS into instantaneous transformer saturation characteristics–implementation in MATLAB/SPS-ST,” *Internat. Review of Electrical Engineering*, vol. 4, no. 2, pp. 367–374, 2019.

[4] S. G. Abdulsalam, W. Xu, W. L. A. Neves, and X. Liu X, “Estimation of transformer saturation characteristics from inrush current waveforms,” *IEEE Trans. Power Delivery*, vol. 21, no. 1, pp. 170–177. Jan. 2006.

[5] A. Ketabi, and M. Naseh, “Single-phase transformer modeling for inrush currents simulation using differential evolution,” *Europ. Trans. Electrical Power*, vol. 22, no. 3, pp. 402–411, Apr. 2012.

[6] R. Oyanagi, T. Noda, and M. Ichikawa, “A Method for estimating the current–flux curve of a single-phase transformer for electromagnetic transient simulations of inrush currents, ”*Elect. Engineering in Japan*, vol. 204, no. 2, pp. 13–24, Jul. 2018.

[7] T. Canal, F. X. Zgainski, and V. L. Renouard, “Determination of the saturation curve of power transformers by processing transient measurements,” in *Proc. 2021 Internat. Conference on Power Systems Transients* (IPST2021), Belo Horizonte, Brazil, pp. 1–7.

[8] M. I. Abdelwanis, A. Abaza, R. A. El-Sehiemy, M. N. Ibrahim, and H. Rezk, “Parameter estimation of electric power transformers using Coyote optimization algorithm with experimental verification,” *IEEE Access*, vol. 8, pp. 50036-50044, Mar. 2020.

[9] M. P. Ćalasan, A. Jovanović, V. Rubežić, D. Mujičić, and A. Deriszadeh, “Notes on parameter estimation for single-phase transformer,” *IEEE Trans. Ind. Appl.*, vol. 56, no. 4, pp. 3710-3718, Jul. –Aug. 2020.

[10] M. I. Mossad, M. Azab, and A. Abu-Siada, “Transformer parameters estimation from nameplate data using evolutionary programming techniques, ”*IEEE Trans. Power Delivery*, vol. 29, no. 5, pp. 2118–2123, Oct. 2014.

[11] IEEE WG on Modeling and Analysis of System Transients Using Digital Programs, “Modeling and analysis guidelines for slow transients – Part III: The study of ferroresonance,” *IEEE Trans. Power Delivery*, vol. 15, no. 1, , pp. 255–265. Jan. 2000.

[12] E. Zia, “Resonance and ferroresonance in power networks,” WG C4.307, CIGRE, pp. 156–161, 2013.

[13] M. Moradi, and A. Gholami, “Numerical and experimental analysis of core loss modeling for period–1 ferroresonance,” *Europ. Trans. Electrical Power*, vol. 21, no. 1, pp. 18–26, Jan. 2011.

[14] I. R. Pordanjani, X. Liang, Y. Wang, and A. Schneider, “Single–phase ferroresonance in an ungrounded system during system energization,” *IEEE Trans. Ind. Appl.*, vol. 57, no. 4, pp. 3530–3537, Jul. –Aug. 2021.

[15] B. Behdani, M. Allahbakhshi, and M. Tajdinian, “On the impact of geomagnetically induced currents in driving series capacitor compensated power systems to ferroresonance,” *Elect. Power and Energy Systems*, vol. 125, pp. 1–19, Feb. 2021.

[16] W. Piasecki, M. Stosur, T. Kuczek, M. Kuniewski, and R. Javora, “Ferroresonance in MV voltage transformers: pragmatic experimental approach towards investigation of risk and mitigating strategy,” in *Proc. 2017 Inernat. Conference on Power Systems Transients* (IPST2017), Seoul, Republic of Korea, pp. 1–5.

[17] R. Ashino, M. Nagase, and R. Vaillancourt, "Behind and beyond the MATLAB ODE suite", Comp. Math. Applications, vol. 40, pp. 491–512, 2000.

[18] A. Tokić, M. Kasumović, M. Pejić, V. Milardić, and T. C. Akinci, “Determination of single-phase transformer saturation characteristic by using Nelder–Mead optimization method,” *Electr. Engineering*, vol. 103, pp. 1321–1333, Jan. 2021.

[19] A. Tokić, and I. Uglešić, “Elimination of overshooting effects and suppression of numerical oscillations in transformer transient calculations,” *IEEE Trans. Power Delivery*, vol. 23, no. 1, pp. 243–251, Jan. 2008.

[20] A. Tokić, and J. Smajić, “Modeling and simulations of ferroresonance by using BDF/NDF numerical methods,” *IEEE Trans. Power Delivery*, vol. 30, no. 1, pp. 342–350, Feb. 2015.

[21] A. Tokić, V. Milardić, I. Uglešić, and A. Jukan, “Simulation of three–phase transformer inrush currents by using backward and numerical differentiation formulae,” *Elect. Power Systems Research*, vol. 127, pp. 177–185, Oct. 2015.

[22] E. Hairer, and G. Wanner, *Solving Ordinary Differential Equations II: Stiff and Differential-Algebraic Problems*. New York, USA: Springer, 2010.

[23] U. Ascher, and L. R. Petzold, *Computer Methods for Ordinary Differential Equations and Differential-Algebraic Equations*. Philadelphia, PA, USA: SIAM, 1998.

[24] J. Nocedal, and S. J, Wright, *Numerical Optimization*, Springer-Verlag, New York, 2006.

[25] A. Rajan, and T. Malakar, “Optimal reactive power dispatch using hybrid Nelder–Mead simplex based firefly algorithm, ”*Elect. Power and Energy Systems*, vol. 66, pp. 9–24, March 2015.

[26] A. Galantai, “Convergence of the Nelder-Mead Method, ”*Numerical Algorithms*, vol. 90, pp. 1043–1072, 2022.

[27] Y. Tanaka, R. Yonezawa, T. Noda, and T. Kikuma, “Application of the Kriging method for an electromagnetic-transient-simulation-aided optimization technique,” in *Proc. 2018 Internat. Conference on Power System Technology* (POWERCON), Guangzhou, China, pp. 2784-2790.

[28] S. Singer, and J. Nelder, “Nelder-Mead Algorithm,” *Computer Science, Scholarpedia*: 2928, Vol. 4, No. 7, July, 2009.